

Low-Complexity Multi-Antenna Coded Caching Using Location-Aware Placement Delivery Arrays

Hamidreza Bakhshzad Mahmoodi, *Student Member, IEEE*, MohammadJavad Salehi, *Member, IEEE*, and Antti Tölli, *Senior Member, IEEE*

Abstract—A location-aware multi-antenna coded caching scheme is proposed for applications with location-dependent data requests, such as wireless immersive experience, where users are immersed in a three-dimensional virtual world. The wireless connectivity conditions vary as the users move within the application area motivating the use of a non-uniform cache memory allocation process to avoid excessive delivery time for users located in wireless bottleneck areas. To this end, a location-aware placement and delivery array (LAPDA) is designed for cache-aided multiantenna data delivery with a fast converging, iterative linear beamforming process. The underlying weighted max-min transmit precoder design enables the proposed scheme to serve users in poor connectivity areas with smaller amounts of data while simultaneously delivering larger amounts to other users. Our new scheme is suitable for large networks due to its linear transceiver structure and it is not constrained by the number of users, cache size, or the number of antennas at the transmitter, unlike the existing schemes. Despite non-uniform cache placement, the proposed scheme still achieves a significant degree of coded caching gain that is additive to the multiplexing gain and greatly outperforms the conventional symmetric CC schemes in terms of both average and 95-percentile delivery time.

Index Terms—Multi-antenna communications, coded caching, location-dependent caching, immersive viewing.

I. INTRODUCTION

Mobile data traffic is exponentially growing, and this trend will continue as the market is constantly inundated with technologies and devices that support new data-intensive applications in different forms and capabilities [1]. Wireless eyewear devices, for example, enable data-intensive mobile extended reality (XR) applications [2], [3], which are also subject to strict quality of service (QoS) requirements such as low latency (< 10 ms) and high data rate transmission (6.37 – 95.55 Gbps) [4]–[9]. This differs greatly from conventional ultra-low latency and low-rate requirements for internet-of-things applications [10]. The low latency, along with the high delivery rates, require more sophisticated transmission methods than those offered by current wireless network standards [6]–[8]. Therefore, to meet the requirements of future wireless XR applications, new delivery schemes with higher bandwidth efficiency are needed.

This work was supported by the Academy of Finland under grants no. 319059 (Coded Collaborative Caching for Wireless Energy Efficiency) and 346208 (6G Flagship program). This article was presented in parts at the IEEE International Conference on Communications (ICC) 2022, Seoul, Korea. (*Corresponding author: Hamidreza Bakhshzad Mahmoodi*). Hamidreza Bakhshzad Mahmoodi, MohammadJavad Salehi and Antti Tölli are with the Centre for Wireless Communications, University of Oulu, FIN-90014 Oulu, Finland. (e-mail:First-Name.Last-Name@oulu.fi)

One possible option, given that upcoming mobile broadband applications rely heavily on asynchronous content reuse [11], is to utilize proactive caching at the end-users to relieve network congestion and bandwidth consumption during peak times [12]. In this regard, various studies have explored proactive caching in single-input single-output (SISO) configurations, demonstrating its benefits for meeting XR application requirements [13]–[16]. Specifically, with the available memory at the end users, the whole or part of the requested content can be cached beforehand and rendered by the end user at the request time. This results in significant bandwidth and delay-reduction gains and alleviates the traffic burden over the wireless network [13]–[16].

Unlike conventional caching schemes that rely on the available memory of each user (see, e.g., [11]–[18]), the coded caching (CC) scheme originally introduced in [19] benefits from the aggregated memory throughout the network. In fact, it enjoys a so-called *global caching* gain, available through careful cache placement and multicast transmissions that results in improved overall performance compared to traditional schemes [11]–[18]. As such, the transmission bandwidth for delay-constrained XR applications has been effectively reduced in SISO setups by leveraging coded cache placement and mobile device computing capabilities [20]. The CC scheme is especially advantageous for large networks as the achievable global caching gain scales linearly with the number of users in the network. This makes it ideal for collaborative XR scenarios where a group of users is served simultaneously within a confined environment, with each user’s individual actions impacting the results perceived by all users (c.f., [2], [21]–[24]). In this regard, a *location-dependent* CC-based cache placement and delivery scheme, originally designed for SISO setups, has been proposed in [21].

In addition, the CC scheme’s ability to combine global caching and spatial multiplexing gains is another critical feature [25]. This is particularly appealing given that multi-antenna connectivity will be a crucial feature of upcoming communication systems [5]. Thus, the SISO setup in [21] has been extended to a multiple-input single-output (MISO) setup in [22]–[24], to benefit from spatial multiplexing and global caching gains simultaneously. In this paper, we intend to overcome some of the practical limitations of our earlier schemes in [22]–[24]. Notably, we propose a new location-dependent CC scheme, suitable for large networks due to its linear transceiver structure, and not constrained by the number of users, cache size, or the number of antennas at the transmitter, unlike the existing schemes.

A. Literature review

Coded caching. The original CC scheme in [19] was intended for SISO setups with an error-free shared link. This work was later extended to more practical scenarios, including multi-server [26] and MISO [25], [27], [28] setups. The early high signal-to-noise ratio (SNR) analysis in [25]–[27] proved that the so-called degrees of freedom (DoF) achieved by the MISO-CC scheme is optimal under uncoded cache placement and single-shot data delivery. Later, the analysis in [28] showed that an optimized multi-antenna precoder design is necessary for the CC scheme to perform well also in the low-SNR regime. Soon, device-to-device (D2D) CC schemes were proposed (e.g., [29]–[31]) to increase the network throughput.

Bit- and signal-level CC. Despite exciting theoretical gains, various practical issues have restricted the real-world implementation of CC schemes. One prominent problem is the exponentially growing file-division requirement (w.r.t the network size), known as the *subpacketization* bottleneck. To address this issue, a combinatorial subfile assignment based on placement delivery arrays (PDA) was proposed in [32]. The PDA structure provides a set of conditions (reviewed for MISO systems in Section III) that allows a given matrix to be used for both content placement and delivery of a CC scheme, thus translating the subpacketization reduction problem to finding a small-dimension matrix satisfying PDA conditions. Interestingly, authors in [32] demonstrated that all the schemes in [19], [25]–[31] could also be presented as PDAs. Motivated by the generalized framework in [32], various PDA-based CC schemes were later proposed for different settings, aiming for reduced subpacketization [33]–[35].

A major breakthrough in subpacketization reduction was achieved with the introduction of *signal-level* CC schemes in [36]. In contrast to *bit-level* CC schemes [19], [25]–[31], where file fragments intended to different users are combined/separated using bit-wise XOR operations in the finite field, signal-level CC schemes rely on the superposition of all precoded data terms in the signal domain and the regeneration and cancellation of the unwanted parts at the physical layer of each receiver (see [2] for a more detailed explanation). As a result, the design flexibility is greatly increased compared with bit-level schemes, enabling the subpacketization requirement of MISO-CC setups to be even smaller than their comparable SISO-CC settings [36]. The signal-level scheme of [36] was then extended to centralized [37] and decentralized [38] shared-cache scenarios where a limited number of cache-enabled helper nodes serve a group of cache-less users. The applicability of signal-level CC schemes was later extended, e.g., to multiple-input multiple-output (MIMO) setups [39], [40], and to dynamic networks wherein users may freely enter/depart the network at will [41]–[43]. Finally, to make the design of signal-level CC schemes more systematic, an enhanced PDA framework, called multi-antenna placement and delivery arrays (MLPDA), was proposed in [44]. Of course, signal-level CC schemes also suffer from drawbacks such as inferior finite-SNR performance compared with bit-level CC schemes [45], [46] and the requirement to regenerate and remove the interference in the physical layer [2]. However,

the remarkable flexibility of signal-level approaches continues to inspire ongoing research endeavors aimed at utilizing them to overcome different implementation challenges encountered in CC schemes.

The near-far effect. Another crucial problem of conventional CC schemes is the *near-far* issue, which affects content delivery applications (e.g., [25]–[35]) in general and XR applications in particular. In CC schemes, a common multicast message is transmitted to serve several users at a time, and all these users must be able to decode the message simultaneously. As a result, the achievable rate is always limited by the user(s) with the worst channel condition. Studies on SISO-CC networks have shown that the practical gains of CC schemes could entirely vanish at the low-SNR region due to the near-far issue [47]. To address this issue, a congestion control technique is proposed in [48] with the intention of avoiding serving users that experience adverse channel conditions altogether. Similar scheduling approaches are also proposed in [49], [50], where joint queue minimization and packet control, as well as power minimization and scheduling, are considered for delay-constrained CC applications. In another work [51], a CC scheme with partial codewords (i.e., with a smaller number of data terms in the codeword compared to the baseline CC scheme of [52]) is introduced to adjust the user-specific QoE based on their current channel conditions.

Multi-rate transmission in CC. In [25]–[38], [44], [53], equal-sized data chunks are combined to form a common message. In contrast, in [54], data terms with different sizes are combined via nested code modulation (NCM), creating codewords that serve every user in the multicasting group at a different rate. Similarly, combining the shared-cache idea of [36] with the NCM of [54], the near-far problem was mitigated in [55], [56]. The proposed system model in [54] assumed fixed link capacities, particularly tailored for backhaul networks. Motivated by the results in [54], a location-dependent CC scheme was proposed in [21] for networks with variable link capacities, particularly applicable for future wireless XR applications. Later, the SISO setting in [21] was extended to a location-dependent MISO setup in [22]–[24]. Specifically, while the schemes in [22], [24] benefit from the NCM for data delivery, the scheme in [23] uses a modified version of the signal-level scheme in [53] to support multi-rate transmission. Nevertheless, the schemes proposed in [22], [24] do not scale well with the increasing number of users. This is attributed to the exponential increase in the number of variables and constraints in the transmit precoder design optimization problem and the complex receiver structure. Similarly, the signal-level scheme proposed in [23] is limited to scenarios where the global caching gain is not greater than the multiplexing gain. Hence, a general framework that can scale with the number of users without such scaling impediments is still missing in the literature.

B. Our Contribution

A novel location-dependent multi-antenna CC scheme is proposed in this paper, leveraging location-aware placement and delivery arrays (LAPDA) formed using a proper set of

MLPDAs (c.f., [44]). In the considered system setup, users are equipped with dedicated cache memories and can roam freely within the application environment. A location-aware, non-uniform memory allocation strategy similar to [24] is employed to ensure that users in areas with poor wireless link quality do not experience excessive delivery times. Due to different amounts of memory allocated to different locations, multiple location-dependent MLPDAs are utilized to define which part(s) of every file should be cached by each user. As a result, the number of cached subfiles for each location-dependent content could be different, and hence, a different transmission schedule may be needed to deliver the missing subfiles requested at each location. To handle this requirement, a file-mapping process is devised where all requested files in different locations are divided into equal numbers of file fragments (of various sizes). A common MLPDA is then used to deliver all requested file segments to all users, regardless of their location.

Parts of this paper have been published in our previous work [23]. In this paper, one important limitation of [23] is addressed, namely the requirement for a larger spatial multiplexing gain than the global caching gain. This limitation arose from the utilization of the CC scheme proposed in [53], which is primarily designed for scenarios with a lower global caching gain relative to the multiplexing gain. To circumvent this limitation, we instead utilize a set of appropriately designed MLPDAs, which are demonstrated to be a general framework for signal-level CC schemes [44], including shared caching-based approaches (e.g., [39], [40], [57]). Serving a large number of concurrent users submerged into a collaborative XR experience within a bounded environment is an ideal scenario for the proposed delivery scheme. In this regard, we follow the XR connectivity framework proposed in our earlier work [24] but utilize a simple linear transceiver design for data delivery with a fast iterative beamforming process through the use of LAPDAs that enable unicast transmissions. In particular, the unicast transmission allows a low-complexity beamformer design based on weighted max-min optimization, which is iteratively solved via Lagrangian duality. This fast beamformer design allows the proposed scheme to be applied to large networks, leading to significantly higher achievable coded caching gains compared to our previous method presented in [24]. This translates into a notable performance advantage over conventional unicasting and multicasting schemes, as demonstrated by simulation results.

C. Notation and structure

Matrices and vectors are presented by boldface upper and lower case letters, respectively, and calligraphic letters are used to denote sets. For the set \mathcal{A} and vector \mathbf{v} , $|\mathcal{A}|$ and $\|\mathbf{v}\|$ represent the cardinality of \mathcal{A} and norm of \mathbf{v} , respectively. For two sets \mathcal{A} and \mathcal{B} , $\mathcal{A} \setminus \mathcal{B}$ includes the elements of \mathcal{A} that are not in \mathcal{B} . Finally, \mathbb{W} denotes the set of non-negative integers, $[m]$ represents the set of integers from 1 to m , and \oplus denotes addition in the corresponding finite field.

The rest of this paper is organized as follows. In section II, we describe our location-based system model. A two-phase

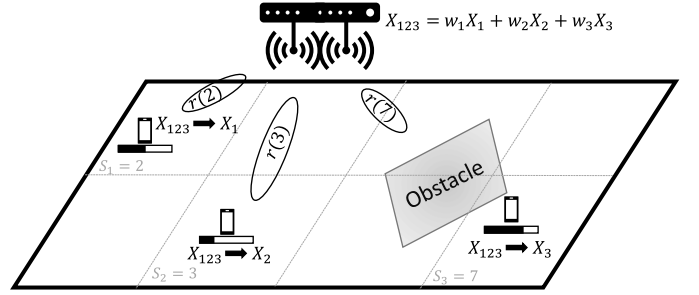


Fig. 1: An application environment with $K = 3$ users, split into $S = 8$ STUs. $r(s)$ is the STU-specific achievable rate and $r(3) > r(2) > r(7)$. X_{123} is the transmitted message, X_i and w_i represents the data part intended for user i and its corresponding precoder, respectively. The black bar below each user indicates how much of the requested data is cached.

cache placement scheme comprised of memory allocation and cache arrangement processes is described in section III, while section IV discusses the delivery procedure. In section IV-B, weighted-max-min beamforming, tailored for the considered location-based cache placement setup, is introduced. In the end, numerical results are provided in section V, while section VI concludes the paper.

II. SYSTEM MODEL

A downlink scenario is considered where a server with L transmit antennas serves K single-antenna, cache-enabled users.¹ The users are located within a bounded environment, such as a gaming hall, an operating room, or an exhibition hall. The system model is quite similar to our previous study in [24] but with new placement and transmission schemes designed to support large networks with improved scalability. Let $\mathcal{K} = [K]$ denote the set of users with limited memory capacities who can navigate within the coverage area. Users are assumed to request data from the server, depending on their location and application requirements. The environment is partitioned into S single transmission units (STU), wherein a distinct 3D image is required to reconstruct the 360-degree spherical virtual viewpoint around the user at each STU [2]. As a small example, Figure 1 represents a simple application environment with eight STUs, where S denotes the set of STUs.

The STU mapping is designed so that the wireless channel quality can be assumed to be almost the same for all points within a given STU. We also assume the 3D image within each STU can be decomposed into *static* and *dynamic* components [2], [24]. An example of such decomposition is shown in Figure 2. A proper modeling structure, such as the one described in [3], would allow users to cache the entire static part and a significant portion of the dynamic part in advance [24]. In this paper, we concentrate on the efficient delivery of this cacheable part of the content.²

¹Here, L refers to the attainable spatial multiplexing gain at the transmitter, which is upper-bounded by the real number of antennas. Nevertheless, ‘antenna count’ is used throughout the text for simplicity.

²Due to the interaction of objects in the virtual world, the BS must also provide control data to aid users in reconstructing the dynamic content. However, such control data is considered to cause a fairly minor overhead and is omitted in this paper.

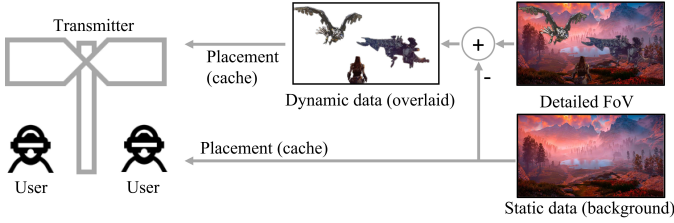


Fig. 2: XR Data decomposition into static and dynamic parts.

Denote $W(s)$ as the (cacheable part of) file required for reconstructing the detailed FoV in STU $s \in \mathcal{S}$ and, without loss of generality, assume $|W(s)| = F$ bits for every $s \in \mathcal{S}$. Unless otherwise stated, this paper considers normalized data units, and F is dropped in subsequent notations. System operation consists of two phases: *cache placement* and *delivery*. During the placement phase, each user k , equipped with a cache memory of size M (normalized) bits, stores a message $Z_k = Z_k(W(s_1), \dots, W(s_S))$ in its cache, where $Z_k(\cdot)$ denotes a function of the files $W(s)$, $\forall s \in \mathcal{S}$, with entropy not larger than M bits.

During the delivery phase, users located within the application environment request missing data from the server to reconstruct the FoV of their current locations. Specifically, a request vector $\mathbf{d} := \{d_k \mid d_k \in \mathcal{S}, \forall k \in \mathcal{K}\}$ is first collected at the BS, where $W_{d_k} \equiv W(s_{d_k})$ is the file requested by user k in STU s_{d_k} . To deliver missing parts of the files in \mathbf{d} , the BS then transmits several precoded messages $\mathbf{x}_{\mathcal{U}}$ at different intervals, where $\mathcal{U} \subseteq \mathcal{K}$ denotes the set of users receiving (a part of) their requested data from $\mathbf{x}_{\mathcal{U}}$. The number of precoded messages (and hence, the number of different user sets \mathcal{U}) depends on the underlying CC scheme. Every message $\mathbf{x}_{\mathcal{U}}$ comprises several unit power codewords x_k , where x_k contains useful data for a user $k \in \mathcal{U}$. Thus, $\mathbf{x}_{\mathcal{U}}$ is built as $\mathbf{x}_{\mathcal{U}} = \sum_{k \in \mathcal{U}} \mathbf{v}_k x_k$, where $\mathbf{v}_k \in \mathbb{C}^L$ denotes the precoding vector dedicated to codeword x_k . To be specific, \mathbf{v}_k is designed to suppress the interference caused by x_k on a subset of users in $\mathcal{I}_k \subset \mathcal{U}$ that can not remove the interference by their cache contents. After the transmission of $\mathbf{x}_{\mathcal{U}}$, every user $k \in \mathcal{U}$ receives

$$y_k = \mathbf{h}_k^H \sum_{k \in \mathcal{U}} \mathbf{v}_k x_k + z_k, \quad (1)$$

where the channel vector between the BS and user k is denoted by $\mathbf{h}_k \in \mathbb{C}^L$, and $z_k \sim \mathcal{CN}(0, N_0)$ represents the additive white Gaussian noise. Note that both the local cache content Z_k and the received signals from the wireless channel over different time intervals are used at the decoder of user k to reproduce the requested file W_{d_k} . Moreover, the instantaneous channel state information at the transmitter (CSIT) is assumed to be available during the *delivery phase*, which is utilized for beamformer design and rate allocation.³

Finally, as discussed in [24], an approximate throughput estimate, e.g., based on the statistics collected from previous application runs, is required for proper location-dependent cache placement. Unlike the delivery phase, it is not possible to calculate instantaneous achievable rates during the

³CSIT measurement is feasible through reciprocal reverse link pilot measurements assuming data delivery is carried out within the channel coherence time. A detailed discussion on CSI acquisition in CC networks can be found in [53].

placement phase. This is because important information such as concurrently scheduled users, their locations, channel conditions, and precoding algorithms is not yet available. The aim of the approximation is to have a relative rate difference among different STUs available to allocate distinct portions of memory to them accordingly. Intuitively, to avoid extensive transmission times for users with poor connectivity, data needed at STUs with the lowest approximated rates should occupy most of the memory. To this end, we use the following rate approximation originally proposed in [24]

$$r(s) = \frac{\Omega}{F} C_p \mathbb{E} \left[\log \left(1 + \frac{P_T \|\mathbf{h}_{k_s}\|^2}{N_0} \right) \right] \quad [\text{files/second}], \quad (2)$$

where C_p is a pre-log scaling factor containing any practical overhead, P_T is the transmission power, Ω is the communication bandwidth, and $\mathbf{h}_{k_s} \in \mathbb{C}^L$ is the channel vector between the server and a user k located in STU s . Note that the expectation is taken over all user locations and channel realizations in STU s (c.f. [24] for more details).

III. CACHE PLACEMENT

A PDA-based location-dependent cache placement scheme comprising two consecutive processes, *memory allocation* and *cache arrangement*, is used in this paper. The memory allocation process is similar to [24] and prioritizes content requested in locations with poor wireless connectivity in order to mitigate excessive delays during the content delivery phase. Given the result of the memory allocation process, the cache arrangement process is then used to clarify what data parts should be cached by each user. One of the key novelties of this paper is the introduction of a PDA-based cache arrangement process that allows the overall scheme to be scalable w.r.t various network parameters. Nevertheless, for clarity, the memory allocation process of [24] is also briefly explained in the following.

Memory allocation [24]: Real-time applications (e.g., XR) typically require a bounded delivery time. Excessive delivery delays can be circumvented by reserving a larger share of memory to store data requested in poor connectivity areas. Accordingly, the memory allocation process specifies the normalized cache size $m(s)$ reserved for storing (a fraction of) each STU-specific file $W(s)$ at every user. This paper assumes no prior knowledge about the users' spatial locations during the subsequent delivery phase; hence, we consider uniform access probability for all STUs during the placement phase.⁴

Following [24], if $m(s)$ values are known, the total delivery time T_T can be approximated as

$$\hat{T}_T = \frac{K}{K\bar{m} + L} \max_{s \in \mathcal{S}} \frac{1 - m(s)}{r(s)} \quad [\text{seconds}], \quad (3)$$

where $\bar{m} = \min_{s \in \mathcal{S}} m(s)$ is the least allocated memory for a STU and $r(s)$ is the approximated rate at STU s (c.f. Eq. (2)). The $K\bar{m} + L$ term in the denominator of (3) approximates the achievable DoF for the non-uniform memory allocation scenario (note that for the uniform allocation, the DoF is upper bounded by $K \frac{M}{S} + L$ [44]), and the term $K \max_{s \in \mathcal{S}} \frac{1 - m(s)}{r(s)}$

⁴The placement efficiency can be further improved by using prior knowledge about the access likelihood for each STU.

approximates the worst-case delivery time across all the STUs when K users are served simultaneously. In order to find approximate $m(s)$ values that minimize the expected delivery time, we first rewrite (3) as $\hat{T}_T = \frac{1}{\bar{m} + \frac{L}{K}} \max_{s \in \mathcal{S}} \frac{1 - m(s)}{r(s)}$, and then, formulate the memory allocation process as the following linear fractional programming (LFP) problem:

$$\begin{aligned} & \min_{m(s), \gamma \geq 0, m \geq 0} \frac{\gamma}{m + \frac{L}{K}} \\ \text{s.t.} \quad & \frac{1 - m(s)}{r(s)} \leq \gamma, \quad \forall s \in \mathcal{S}, \\ & m \leq m(s), \quad \forall s \in \mathcal{S}, \quad \sum_{s \in \mathcal{S}} m(s) \leq M. \end{aligned} \quad (4)$$

Note that at the optimal solution to (4), $m = \bar{m} = \min_{s \in [S]} m(s)$.

Using the Charnes-Cooper transformation, the LFP in (4) can be reformulated as a linear programming problem and solved efficiently [24]. For ease of exposition, we assume that $Km(s)$ is a positive integer for all $s \in \mathcal{S}$ throughout the text. The non-integer $Km(s)$ case is addressed in Appendix B using time-sharing, which is an alternative method that surpasses the performance of the approach proposed in [24].

Cache arrangement: We utilize a location-aware placement delivery array (LAPDA) to store data fragments of files in users' cache memories. Let \mathcal{Q} denote a specific LAPDA consisting of a set of S STU-specific MLPDA matrices $\mathbf{Q}_s, s \in \mathcal{S}$, that are interrelated with an extra cross-matrix condition that ensures data delivery is possible with the given non-uniform memory allocation. Before going through a detailed explanation of LAPDA, let us first review the general definition of MLPDAs.

Definition 1. A (L, K, F_s, Z_s, N_s) MLPDA $\mathbf{Q}_s = [\mathbf{Q}_s(f_s, k)]$, $f_s \in [F_s]$, $k \in [K]$, is a $F_s \times K$ matrix whose elements include the specific symbol "*" and N_s positive integers $\{1, 2, \dots, N_s\}$. For positive integers L, K, F_s , and Z_s , \mathbf{Q}_s satisfies [44]:

- C1. The symbol "*" appears Z_s times in each column, such that $\frac{Z_s}{F_s} = m(s)$;
- C2. Each integer $n \in [N_s]$ appears at least once in the matrix;
- C3. Each integer appears at most once in each column;
- C4. For every $n \in N_s$, if we define $\mathcal{U}(n, s) := \{k \mid \exists f_s \in [F_s], \mathbf{Q}_s(f_s, k) = n\}$, $\mathcal{F}(n, s) := \{f_s \mid \exists k \in [K], \mathbf{Q}_s(f_s, k) = n\}$, and \mathbf{Q}_s^n to be a sub-matrix of \mathbf{Q}_s comprised of all rows and columns containing n (i.e., $\mathbf{Q}_s^n = [\mathbf{Q}_s(f_s, k)]$, $f_s \in \mathcal{F}(n, s)$, $k \in \mathcal{U}(n, s)$), the number of integer entries in each row of \mathbf{Q}_s^n is less than or equal to L , i.e., $|\{k \mid k \in \mathcal{U}(n, s), \mathbf{Q}_s^n(f_s, k) \in [N_s]\}| \leq L, \forall f_s \in \mathcal{F}(n, s)$.

As discussed in [44], the (L, K, F_s, Z_s, N_s) MLPDA \mathbf{Q}_s uniquely identifies a placement-delivery strategy for a MISO network with K cache-enabled users, a coded caching gain of $t_s = Km(s)$, and a spatial multiplexing gain of L . In this regard, each file is first divided into F_s subpackets, from which all subpackets $f_s \in [F_s]$ are stored by all users $k \in [K]$ if $\mathbf{Q}_s(f_s, k) = *$. The delivery phase then consists of N_s transmissions, where at transmission $n \in [N_s]$, subpackets $f_s \in \mathcal{F}(n, s)$ are sent to users $k \in \mathcal{U}(n, s)$ if $\mathbf{Q}_s(f_s, k) = n$.

Algorithm 1 Location-based cache placement

```

1: procedure MEMORY_ALLOCATION
2:   Find  $\{m(s)\}$  by solving Eq. (4)
3: procedure CACHE_ARRANGEMENT
4:   for all  $s \in \mathcal{S}$  do
5:      $W(s) \rightarrow \{W_f(s) \mid \forall f \in [F_s]\}$ 
6:     for all  $f \in [F_s]$  do
7:       for all  $k \in \mathcal{K}$  do
8:         if  $\mathbf{Q}_s(f, k) = *$  then
9:           Put  $W_p(s)$  in the cache of user  $k$ 

```

Note that condition C1 ensures that the memory constraints are met, C2 prevents empty transmission, C3 removes the need for successive interference cancellation (SIC), and C4 ensures that any interference that cannot be removed with cache content is suppressed by a proper precoder.

For the proposed location-dependent cache placement where each STU $s \in \mathcal{S}$ has a possibly different allocated memory portion $m(s)$, it is necessary to use a different MLPDA \mathbf{Q}_s for each state to satisfy the memory constraint. This is different from conventional MLPDA schemes that use a single MLPDA to store all library files. In fact, given a set of MLPDAs $\{\mathbf{Q}_s\}$, the files for every STU $s \in \mathcal{S}$ are first divided into F_s subfiles, where F_s can vary for each STU. Then, for every STU $s \in \mathcal{S}$, every user $k \in \mathcal{K}$ caches all subfiles $f_s \in [F_s]$ if $\mathbf{Q}_s(f_s, k) = *$. Algorithm 1 summarises the placement process for a set of MLPDA $\{\mathbf{Q}_s\}$.

Using a distinct \mathbf{Q}_s for each STU results in an unequal number of subfiles F_s , number of cached data elements Z_s , and time slots N_s to deliver location-dependent missing data. Hence, an additional cross-matrix condition is added to the conventional MLPDA definition to ensure a feasible delivery scheme for the proposed non-uniform placement. Accordingly, a proper LAPDA \mathcal{Q} is defined as follows.

Definition 2. A $(L, K, \{F_s\}, \{Z_s\}, \{N_s\})$ LAPDA \mathcal{Q} is a set of S number of (L, K, F_s, Z_s, N_s) MLPDAs \mathbf{Q}_s where for every $(s, \hat{s}) \in \mathcal{S}$ for which $m(s) > m(\hat{s})$ we have

$$\begin{aligned} \forall f_{\hat{s}} \in [F_{\hat{s}}], \exists f_s \in [F_s] : \mathcal{B}_{f_{\hat{s}}} \subseteq \mathcal{B}_{f_s}, \\ \forall f_s \in [F_s], \exists f_{\hat{s}} \in [F_{\hat{s}}] : \mathcal{B}_{f_s} \subseteq \mathcal{B}_{f_{\hat{s}}}, \end{aligned}$$

where $\mathcal{B}_{f_s} = \{k \mid k \in [K], \mathbf{Q}_s(f_s, k) = *\}$ is the set of columns including * in their f_s 'th row.

The following example illustrates the entire cache placement process, including memory sharing and cache arrangement. In Section IV, we propose a novel delivery algorithm tailored for the above described non-uniform cache placement that achieves a significant coded caching gain, similar to the location-dependent scheme of [24], but now applicable to much larger networks. Moreover, in Appendix A, we discuss how the extra condition in Definition 2 ensures the feasibility of the delivery scheme.

Example 1. To illustrate the proposed location-dependent cache placement, we consider an example scenario from [24] with $K = 4$ users and $L = 2$ transmit antennas. The environment is split into $S = 5$ STUs, and for each STU, the required data size is $F = 400$ Megabytes. Each user has a cache size of 900 Megabytes; hence, the normalized cache size is $M = 2.25$ data units. The approximated normalized

	$s=1$	$s=2$	$s=3$	$s=4$	$s=5$
$r(s)$	3×10^3	2×10^3	1×10^3	2×10^3	3×10^3
$m(s)$	0.25	0.5	0.75	0.5	0.25

TABLE I: Location-specific rate and memory allocation for Example 1.

throughput value for each STU is as given in Table I, where the memory allocation resulting from solving (4) is also shown.

Consider the following MLPDA matrices \mathbf{Q}_1 - \mathbf{Q}_5 , which satisfy the conditions in Definition 1 for the resulting $m(s)$ values in Table I:

$$\mathbf{Q}_1 = \begin{pmatrix} * & 1 & 1 & 2 \\ * & 3 & 2 & 3 \\ * & 6 & 8 & 10 \\ * & * & 4 & 4 \\ 1 & 5 & * & 6 \\ 6 & * & 9 & 11 \\ 2 & 7 & 4 & * \\ 7 & 8 & * & 7 \\ 8 & 9 & * & 12 \\ 3 & 5 & 7 & * \\ 10 & 10 & 11 & * \\ 12 & 11 & 12 & * \end{pmatrix}, \mathbf{Q}_2 = \begin{pmatrix} * & 2 & 1 \\ 1 & * & 2 \\ 2 & 1 & * \\ * & 2 & 1 \end{pmatrix}, \mathbf{Q}_3 = \begin{pmatrix} * & * & * & 1 \\ * & 1 & * & * \\ * & * & 1 & * \\ * & * & * & 1 \end{pmatrix}, \quad (5)$$

$\mathbf{Q}_4 = \mathbf{Q}_2$, and $\mathbf{Q}_5 = \mathbf{Q}_1$. It can be seen that \mathbf{Q}_1 - \mathbf{Q}_5 form a LAPDA according to Definition 2, and hence, can be utilized for location-dependent data delivery. In this regard, using \mathbf{Q}_1 - \mathbf{Q}_5 for the data placement, files $W(1)$ and $W(5)$ are first divided into 12 subfiles, from which 3 are cached in each user's memory. Similarly, files $W(2)$ and $W(4)$ are divided into 4 subfiles, and 2 of them are cached in the memory of each user. Finally, the file $W(3)$ is divided into 4 subfiles, from which 3 are cached in each user's memory.

IV. CONTENT DELIVERY

During the delivery phase, users move within the application environment (hence, change their locations) over time. In each time instance, users reveal their location-dependent file requests to the server.⁵ Without loss of generality, we consider a specific time slot, where every user k in STU s_k requests the file $W_{d_k} \equiv W(s_k)$ from the server to reconstruct its STU-specific FoV. Accordingly, the server builds and transmits several precoded messages to the requesting users. To reconstruct $W(s_k)$, user k requires one normalized data unit, from which a portion of size $m_k \equiv m(s_k)$ units is available in its cache and the remaining part should be delivered by the server. Note that the conventional PDA-based delivery schemes are suited for scenarios where all users cache the same amount of data (e.g., [36], [44], [53]). So, they do *not* apply to our case where users have cached different amounts of their requested files.

A. PDA-based Delivery

To tackle the challenge posed by uneven memory allocation, we first make a temporary assumption that all users have cached the same portion of $\hat{m} = \min_{k \in \mathcal{K}} m_k$ of their requested files, and use any conventional PDA-based delivery scheme in the literature (e.g., [36], [44], [53]) to generate a set of preliminary transmission vectors (PTVs). These vectors are subsequently adjusted to accommodate the different file-indexing procedures employed for STU-dependent cache placement during the placement phase. Using the 'min' operation can limit the performance in certain scenarios when a subset of users have relatively smaller $m(s_k)$ values compared to the rest, e.g., as they are close to the transmitter. To address

⁵Using dynamic CC techniques [41]–[43], this system model can be easily modified to the case only a subset of users reveal their requests in each instant.

such cases, the concept of *phantom users* has been proposed in [24] to separately serve users with small $m(s_k)$ value via unicasting. However, in larger networks considered in this paper, such scenarios are less probable. This is due to the variable m in the LFP formulation (4), which inhibits assigning small values to any $m(s)$, especially when the ratio L/K is small (e.g., for $K \gg L$ case considered in this paper).

For clarity, we designate $\check{\mathbf{x}}_{\mathcal{U}}$ to represent a PTV, which will be later modified to form the transmission vector $\mathbf{x}_{\mathcal{U}}$. In order to build $\check{\mathbf{x}}_{\mathcal{U}}$, we use the MLPDA $\hat{\mathbf{Q}}$ corresponding to the location of the user with the least available memory, i.e., $\hat{\mathbf{Q}} \equiv \mathbf{Q}_{s_{k^*}}$, $k^* := \arg \min_{k \in \mathcal{K}} m(s_k)$. This means we need $\hat{N} = N_{s_{k^*}}$ consecutive transmissions, and the PTV at time instant $n \in [\hat{N}]$ is given as

$$\check{\mathbf{x}}(n) \equiv \check{\mathbf{x}}_{\mathcal{U}(n)} = \sum_{k \in \mathcal{U}(n)} \mathbf{v}_k(n) W_{\check{f}_k^n}(s_k), \quad (6)$$

where

$$\mathcal{U}(n) := \{k \mid \exists \check{f}_k^n \in [F_{s_{k^*}}], \hat{\mathbf{Q}}(\check{f}_k^n, k) = n\} \quad (7)$$

is the set of users served in the n 'th transmission, \check{f}_k^n is the temporary index of the subfile destined to user $k \in \mathcal{U}(n)$, and $\mathbf{v}_k(n)$ is the optimized beamforming vector dedicated to user k . Specifically, $\mathbf{v}_k(n)$ is designed to suppress $W_{\check{f}_k^n}(s_k)$ at every user in the interference indicator set

$$\mathcal{I}_k(n) = \{j \mid j \in \mathcal{U}(n) \setminus k, \hat{\mathbf{Q}}(\check{f}_k^n, j) \neq *\}. \quad (8)$$

In fact, $\mathcal{I}_k(n)$ includes all users $j \in \mathcal{U}(n) \setminus k$ that do not have $W_{\check{f}_k^n}(s_k)$ available in their cache.

Since $\check{\mathbf{x}}(n)$ is built using matrix $\hat{\mathbf{Q}}$ but data placement is done using the set of matrices \mathbf{Q}_s , the temporary index \check{f}_k^n may *not* coincide with the missing subfiles of the files requested by every user $k \in \mathcal{U}(n)$. Example 2 clarifies this statement.

Example 2. Consider the network in Example 1, for which the cache placement is given in (5). Consider a specific time instant n with the following user-to-STU associations: $s_1 = 1$, $s_2 = 2$, $s_3 = 3$, and $s_4 = 4$. Denoting the set of requested sub-files for user k with \mathcal{M}_k and assuming $A \equiv W(1)$, $B \equiv W(2)$, $C \equiv W(4)$, $D \equiv W(5)$, we have

$$\begin{aligned} \mathcal{M}_1 &= \{A_4, A_5, A_6, A_7, A_8, A_9, A_{10}, A_{11}, A_{12}\}, \\ \mathcal{M}_2 &= \{B_3, B_4\}, \quad \mathcal{M}_3 = \{C_4\}, \quad \mathcal{M}_4 = \{D_1, D_2\}. \end{aligned} \quad (9)$$

Note that the subfiles of A, B, C, D are $1/12, 1/4, 1/4, 1/4$ data units in size, respectively. Here, the minimum available amount of the requested data in cache belongs to user 1; hence, $\hat{\mathbf{Q}} \equiv \mathbf{Q}_1$, and we serve all users in $\hat{N} = N_{s_1} = 12$ time slots. For example, the first PTV is built as

$$\check{\mathbf{x}}(1) = \mathbf{v}_1(1)A_4 + \mathbf{v}_2(1)B_1 + \mathbf{v}_3(1)C_1,$$

and the rest can be built accordingly. Now, considering $\check{\mathbf{x}}(1)$, temporary file indices for users 1, 2, and 3 are 4, 1, and 1, respectively. However, from (9), users 2 and 3 already have B_1 and C_1 in their cache memories. Hence, we must carry out an appropriate index mapping process in PTVs before transmission. As a side note, using (8), one can easily verify that the interference indicator sets for PTV $\check{\mathbf{x}}(1)$ are $\mathcal{I}_1(1) = 3$, $\mathcal{I}_2(1) = 3$, and $\mathcal{I}_3(1) = 2$.

To adjust temporary file indices in PTVs, we first note that every user k appears $\hat{F} - \hat{Z}$ times in all PTVs, where $\hat{Z} \equiv Z_{s_{k^*}}$ and $\hat{F} \equiv F_{s_{k^*}}$. However, in practice, every user k needs $F_{s_k} -$

Algorithm 2 File-Fragment Index Matrix

```

1: function INDEX-GENERATOR( $\{\mathbf{G}_k\}, \hat{\mathbf{Q}}$ )
2:   for all  $k \in [K]$  do
3:      $\mathbf{P}_k \leftarrow \mathbf{0}$ 
4:   for all  $n \in [\hat{N}]$  do
5:     for all  $k \in \mathcal{U}(n)$  do
6:        $\chi \leftarrow \hat{f}_k^n$ 
7:       for all  $m \in [\alpha]$  do
8:         for all  $\omega \in [F_{s_k}]$  do
9:           if  $g_{\chi, \omega, k} > 0$  then
10:             $\mathbf{P}_k(n, m) \leftarrow \omega$ 
11:             $g_{\chi, \omega, k} \leftarrow g_{\chi, \omega, k} - 1$ 
12:            Break;
13:   return  $\{\mathbf{P}_k\}$ 

```

Z_{s_k} subfiles to construct its FoV. Hence, to uniformly map the missing subfile indices $f_{s_k} \in [F_{s_k}]$ into temporary PTV indices $\check{f}_k^n \in [\hat{F}]$, we need to divide each subfile into $D_k = \alpha \frac{\hat{F} - \hat{Z}}{F_{s_k} - Z_{s_k}}$ file-fragments, where α is a normalizing coefficient guaranteeing D_k is an integer for every user k (for example, we may set α to be the smallest common multiplier of all $F_{s_k} - Z_{s_k}$ values). We use $W_{f_s}^\phi(s_k)$, $\phi \in [D_k]$, to represent the file-fragments resulting from subfile $W_{f_s}(s_k)$.

After the division of subfiles into file-fragments, the transmission vectors $\mathbf{x}(n)$ are obtained from PTVs $\check{\mathbf{x}}(n)$ by replacing each subfile $W_{\check{f}_k^n}(s_k)$ with $\prod_{m \in [\alpha]} \left(W_{\mathbf{P}_k(n, m)}^q(s_k) \right)$, where

\prod denotes bit-wise concatenation, \mathbf{P}_k is the $\hat{N} \times \alpha$ user-specific file-fragment index matrix (explained shortly), and $q(W_{\mathbf{P}_k(n, m)}(s_k))$ represents the file-specific counter corresponding to the q 'th fragment of the file $W_{\mathbf{P}_k(n, m)}(s_k)$. After initializing with $q = 1$, it is incremented by one each time a fragment of $W_{\mathbf{P}_k(n, m)}(s_k)$ is assigned to the transmission vector. Finally, $\mathbf{x}(n)$ is expressed as

$$\mathbf{x}(n) = \sum_{k \in \mathcal{U}(n)} \mathbf{v}_k(n) \prod_{m \in [\alpha]} \left(W_{\mathbf{P}_k(n, m)}^q(s_k) \right). \quad (10)$$

Matrix elements $\mathbf{P}_k(n, m) \in [F_{s_k}]$ are designed such that 1) all the missing subfiles are delivered to all the users and 2) the cache-aided interference cancellation is performed correctly. To build \mathbf{P}_k , we first form K user-specific File-Mapping (FM) matrices $\mathbf{G}_k, \forall k \in [K]$, with size $\hat{F} \times F_{s_k}$, to map missing subfile indices to temporary PTV indices. Denoting the i 'th row and j 'th column of the matrix \mathbf{G}_k by $g_{i, j, k}$, it represents the number of file-fragments of the subfile $W_j(s_k)$ that should be included in the concatenation process while building $\mathbf{x}(n)$ in (10), if the corresponding PTV $\check{\mathbf{x}}(n)$ includes $W_i(s_k)$ (recall that $j \in [F_{s_k}]$ and $i \in [\hat{F}]$). Accordingly, the FM matrices $\mathbf{G}_k, k \in [K]$ are defined as follows:

Definition 3. A user-specific FM matrix $\mathbf{G}_k = [g_{i, j, k}], \forall i \in [\hat{F}], j \in [F_{s_k}], k \in [K]$ is a $\hat{F} \times F_{s_k}$ matrix whose elements are comprised of non-negative integers, and satisfy the followings:

C1. Denoting the temporary index set (TIS) of user k as $\check{\mathcal{N}}_k$ (i.e., $|\check{\mathcal{N}}_k| = \hat{F} - \hat{Z}$), every row of \mathbf{G}_k not included in $\check{\mathcal{N}}_k$ should be zero, i.e.,

$$g_{i, j, k} = 0, \quad \forall k \in [K], \forall i \in [\hat{F}] \setminus \check{\mathcal{N}}_k, \forall j \in [F_{s_k}].$$

C2. For every user k , denoting the set of its missing subfile indices in STU s_k as a requested index set (RIS) \mathcal{N}_k (i.e.,

Algorithm 3 Location-aware Content Delivery

```

1: procedure DELIVERY( $\{\mathbf{Q}_k\}$ )
2:    $k^* = \arg \min_{k \in \mathcal{K}} m_k$ 
3:    $\hat{\mathbf{Q}} \leftarrow \mathbf{Q}_{k^*}$ 
4:    $\mathbf{q} \leftarrow \mathbf{0}$ 
5:   for all  $k \in [K]$  do
6:     Form  $\mathbf{G}_k$  based on  $\hat{\mathbf{Q}}$ 
7:     Compute  $\mathbf{P}_k$  based on  $\mathbf{G}_k$  using Algorithm 2
8:   for all  $n \in [\hat{N}]$  do
9:      $\mathbf{x}(n) \leftarrow \mathbf{0}$ 
10:    for all  $k \in \mathcal{U}(n)$  do
11:       $x_k \leftarrow 0$ 
12:      for all  $m \in [\alpha]$  do
13:         $p \leftarrow \mathbf{P}_k(n, m)$ 
14:         $\mathbf{q}(W_p(s_k)) \leftarrow \mathbf{q}(W_p(s_k)) + 1$ 
15:         $\chi \leftarrow \mathbf{q}(W_p(s_k))$ 
16:         $x_k \leftarrow \prod (x_k, W_p^\chi(s_k))$ 
17:       $\mathbf{x}(n) \leftarrow \mathbf{x}(n) + \mathbf{v}_k(n)x_k$ 
18:    Transmit  $\mathbf{x}(n)$ 

```

$|\mathcal{N}_k| = F_{s_k} - Z_{s_k}$), every column of \mathbf{G}_k not included in \mathcal{N}_k should be zero, i.e.,

$$g_{i, j, k} = 0, \quad \forall k \in [K], \forall j \in [F_{s_k}] \setminus \mathcal{N}_k, \forall i \in [\hat{F}].$$

C3. Based on Definition 1, each temporary index $i \in \check{\mathcal{N}}_k$ appears only once in PTVs. However, every user k needs a total number of $D_k(F_{s_k} - Z_{s_k}) = \alpha(\hat{F} - \hat{Z}) = \alpha|\check{\mathcal{N}}_k|$ file-fragments. Thus, α file-fragments must be considered for the concatenation process in (10), i.e.,

$$\sum_{j \in \check{\mathcal{N}}_k} g_{i, j, k} = \alpha, \quad \forall k \in [K], \forall i \in \check{\mathcal{N}}_k.$$

C4. As discussed above, each missing subfile of user k is divided into D_k file-fragments. To make sure that all these file-fragments are delivered, the sum of the elements in every column of \mathbf{G}_k that is included in RIS must be equal to D_k , i.e.,

$$\sum_{i \in \mathcal{N}_k} g_{i, j, k} = D_k, \quad \forall k, \forall j \in \mathcal{N}_k.$$

The conditions C1-C4 in Definition 3 constitute a system of equations that needs to be solved to obtain the matrix \mathbf{G}_k . The details of creating and solving this system of equations are provided in Appendix A.

Once $\{\mathbf{G}_k\}$ matrices are found, we can use Algorithm 2 to build $\{\mathbf{P}_k\}$. In a nutshell, in each round (indexed by $n \in [\hat{N}]$ and $m \in [\alpha]$), if $g_{\check{f}_k^n, \omega, k}$ is positive, a file-fragment of $W_\omega(s_k), k \in \mathcal{U}(n)$ is assigned to $\mathbf{P}_k(n, m)$ and $g_{\check{f}_k^n, \omega, k}$ is subtracted by 1 for the following rounds. The whole delivery process is summarized in Algorithm 3, and a clarifying example is provided in the following.

Example 3. Consider the network in Example 2, with the set of requested subfiles for each user (\mathcal{M}_1 - \mathcal{M}_4) given in (9). Following Definition 3, the TIS (the set of temporary indices) of each user can be written as $\check{\mathcal{N}}_1 = \{4, 5, 6, 7, 8, 9, 10, 11, 12\}$, $\check{\mathcal{N}}_2 = \{1, 2, 3, 7, 8, 9, 10, 11, 12\}$, $\check{\mathcal{N}}_3 = \{1, 2, 3, 4, 5, 6, 10, 11, 12\}$, and $\check{\mathcal{N}}_4 = \{1, 2, 3, 4, 5, 6, 7, 8, 9\}$, while the RIS (the set of missing subfile indices) for each user is given as $\mathcal{N}_1 = \{4, 5, 6, 7, 8, 9, 10, 11, 12\}$, $\mathcal{N}_2 = \{3, 4\}$, $\mathcal{N}_3 = \{4\}$ and $\mathcal{N}_4 = \{1, 2\}$. Note that while the TIS is the same size for all users, the size of the RIS can be different. To map each RIS into its corresponding TIS, we first need to divide

$\exp(\bar{\gamma}) \leq (1 + \gamma_k)^{\frac{1}{c_k}}$, we can express the weighted-max-min (WMM) beamforming problem as:

$$\begin{aligned} & \max_{\{\mathbf{v}_k(n), \gamma, \gamma_k\}} \gamma \\ & \text{s.t.} \\ & \gamma^{c_k} - 1 \leq \gamma_k, \quad \forall k \in \mathcal{U}(n), \\ & \gamma_k \leq \frac{|\mathbf{h}_k^H \mathbf{v}_k(n)|^2}{\sum_{i \in \mathcal{I}_k(n)} |\mathbf{h}_k^H \mathbf{v}_i(n)|^2 + N_0}, \quad \forall k \in \mathcal{U}(n), \\ & \sum_{k \in \mathcal{U}(n)} \|\mathbf{v}_k(n)\|^2 \leq P_T, \end{aligned} \quad (15)$$

where P_T is the transmit power and $\gamma = \exp(\bar{\gamma})$. The quasi-convex problem (15) is similar to the one discussed in [53], but with additional convex constraints $\gamma^{c_k} - 1 \leq \gamma_k, \forall k \in \mathcal{U}(n)$.⁶ This problem can be optimally solved by conducting a search over γ using bisection and applying the Lagrangian duality (LD) scheme in [53] for a fixed $\gamma_k = \gamma^{c_k} - 1$.

The LD scheme is an iterative fast-beamforming method used for linear-beamformer design in the literature (c.f., [53] and the references therein). Since it has already been thoroughly described in [53], we will briefly review the LD scheme and its modifications for our WMM optimization. Specifically, we iteratively determine the optimal value of γ using a bisection search, where $\gamma_k = \gamma^{c_k} - 1$. Once γ is fixed, we employ the fixed point iteration method [53] to obtain the dual variables ν_k for $\forall k \in \mathcal{U}(n)$. Specifically, in the initial step, we initialize ν_k as $\nu_k \leftarrow \nu_k[1]$. Subsequently, we iteratively update the dual variables until the desired level of convergence is attained. For each iteration $\tau + 1$, the dual variable ν_k is updated according to the following:

$$\nu_k(\tau + 1) = (\gamma^{c_k} - 1) (\mathbf{h}_k^H \mathbf{\Sigma}_k^{-1}(\tau) \mathbf{h}_k)^{-1}, \quad (16)$$

where $\mathbf{\Sigma}_k(\tau) = \sum_{\hat{k} \in \mathcal{I}_k(n)} \nu_{\hat{k}}(\tau) \mathbf{h}_{\hat{k}} \mathbf{h}_{\hat{k}}^H + N_0 \mathbf{I}$. When (16) is converged, the normalized beamformer $\bar{\mathbf{v}}_k(n), \forall k \in \mathcal{U}(n)$, is calculated as $\bar{\mathbf{v}}_k(n) = \mathbf{\Sigma}_k^{-1} \mathbf{h}_k / \|\mathbf{\Sigma}_k^{-1} \mathbf{h}_k\|$, where $\mathbf{\Sigma}_k = \sum_{\hat{k} \in \mathcal{I}_k(n)} \nu_{\hat{k}} \mathbf{h}_{\hat{k}} \mathbf{h}_{\hat{k}}^H + N_0 \mathbf{I}$. To determine the power vector of the beamformers, denoted by $\tilde{\mathbf{p}}$, we can follow the same steps as presented in [53, Eq.(26)]. Note that γ will be updated based on $\tilde{\mathbf{p}}$ to satisfy the power constraint P_T . Hence, the set of optimal downlink beamformers is computed as $\mathbf{v}_k(n) = \sqrt{p_k} \bar{\mathbf{v}}_k(n)$, where p_k is the k 'th entry of $\tilde{\mathbf{p}}$.

Remark 1. Similar to [24], the proposed WMM beamforming in (15) results in proportional rate allocation such that $\frac{\log(1+\gamma_k)}{\log(1+\gamma_{\bar{k}})} = \frac{c_{\bar{k}}}{c_k}, \forall (k, \bar{k}) \in \mathcal{U}(n)$. However, unlike [24], the proposed delivery scheme in this paper removes the need for successive interference cancellation (SIC) at the receiver. Herein, the SIC requirement is removed due to condition C3 in Definition 1, which prevents multiple message transmissions to a single user at a time. This paper proposes a scheme that is more suitable for large networks, not only because of its simplified transceiver design, but also because of its reduced processing requirements for signal-level delivery, decreased subpacketization [43], and the ability to employ shared caching concepts [37], [38], [42].

⁶Note that γ^{c_k} is convex for $c_k \geq 1$. Since $\{c_k\}$ are just considered as weights for rate allocation purposes, they can be easily replaced by $\{c_k \leftarrow c_k / \min_{k \in [K]} c_k\}$ to make γ^{c_k} a convex function.

Now, using Eq. (13), the total transmission time T_T for the whole delivery process can be calculated as

$$T_T = \frac{1}{\hat{F} - \hat{Z}} \sum_{n \in [\hat{N}]} \max_{k \in \mathcal{U}(n)} \frac{1 - m_k}{\log(1 + \gamma_k)}. \quad (17)$$

It is imperative to note that the calculation of the total transmission time T_T in equation (17), relies on knowing the beamformers for all \hat{N} transmissions, which in turn requires accurate information about user locations and channel conditions. However, during the placement phase, the actual user locations and channel states are unknown, rendering T_T computation infeasible. To address this challenge, we adopt an approximation for T_T for placement purposes that assumes a uniform access probability for all STUs. This approximation is in accordance with the findings presented in [24] and is based on the delivery in Section IV. Thus, the same approximation as in [24] is obtained in this paper, despite the utilization of different delivery and placement techniques.

Lemma 1. The total delivery time T_T calculated in (17) can be approximated as

$$\hat{T}_T = \frac{K}{K\hat{m} + L} \max_{s \in \mathcal{S}} \frac{1 - m(s)}{r(s)}. \quad (18)$$

Proof. We first substitute $\log(1 + \gamma_k)$ in (17) with its upper bound $r(s_k)$ given in (2) to get

$$T_T \sim \frac{1}{\hat{F} - \hat{Z}} \sum_{n \in [\hat{N}]} \max_{k \in \mathcal{U}(n)} \frac{1 - m_k}{r(s_k)}. \quad (19)$$

Then, using inequality $\max_{k \in \mathcal{U}(n)} \frac{1 - m(s_k)}{r(s_k)} \leq \max_{s \in \mathcal{S}} \frac{1 - m(s)}{r(s)}$, we substitute the RHS of (19) with its upper bound to get $T_T \sim \frac{\hat{N}}{\hat{F} - \hat{Z}} \max_{s \in \mathcal{S}} \frac{1 - m(s)}{r(s)}$. Note that $\frac{\hat{N}}{\hat{F} - \hat{Z}} = \frac{K}{K(\hat{F} - \hat{Z})}$, where $\frac{K(\hat{F} - \hat{Z})}{N}$ is nothing but the sum-DoF [44]. Hence, approximating $\frac{K(\hat{F} - \hat{Z})}{N}$ with its upper bound $K\hat{m} + L$ [44], we have

$$T_T \sim \frac{K}{K\hat{m} + L} \max_{s \in \mathcal{S}} \frac{1 - m(s)}{r(s)}. \quad (20)$$

Note that $\hat{m} = \min_{k \in [K]} m(s_k)$ requires user location knowledge, which is unknown during the placement phase. Thus, replacing \hat{m} with its lower bound \bar{m} , (18) is achieved. \square

V. SIMULATION RESULTS

To evaluate the proposed location-dependent scheme, we conduct numerical simulations in a scenario similar to the one studied in [24], albeit with a much larger number of users K .⁷ Specifically, we consider a 30×30 [m²] XR application environment, where a unique 3D image is required at each STU of size 1×1 [m²] to reconstruct a detailed FoV (resulting in a total number of $S = 900$ STUs). A transmitter with L antennas is located on the ceiling, 5[m] above the floor, in the middle of the room. We assume that the small-scale fading of the channel vectors \mathbf{h}_k follows a Rayleigh distribution and use the path loss model of [24] for a user at STU $s \in [S]$:

$$PL(s) = 32.4[dB] + 20 \log_{10}(f) + 10\eta \log_{10}(d_s) + \zeta,$$

⁷The number of users in [24] is limited to nine due to the complex transceiver design and the large subpacketization requirement. Of course, it provides an improved multicasting gain by serving multiple users with a single message.

where d_s represents the distance between the center of STU s and the transmitter, $\eta = 3$ is the pass-loss exponent, and f denotes the frequency. To simulate the effect of randomly placed objects that can obstruct the propagation path between the transmitter and receivers, we use the term $\zeta \sim \mathbb{N}(0, \sigma)$, where σ is the standard deviation. Note that ζ is similar to the shadowing effect observed in outdoor propagation environments. We calculate the expected delivery rates $r(s)$ for the initial memory allocation in (4) by averaging over the rate values for all possible user locations and channel realizations in a given STU (c.f., Eq. (2)). Without considering the shadowing effect ζ , the transmit power is assumed to provide a 5[dB] SNR at the room boundaries, (unless mentioned otherwise). During the delivery phase, optimized weighted max-min beamformers (15) are used, and users are assumed to be located at any STU with equal probability.

Due to the stringent requirement of XR applications for a bounded delivery time, we use the 95-percentile of expected delivery time as a key performance metric (see [24]). We evaluate four distinct placement and delivery schemes:

- **Single-user placement, w/o CC:** This scheme employs a memory allocation process similar to [21] that maximizes the local caching gain at bottleneck areas (equivalent to (4), when the denominator of the objective function is ignored). Data transmission is done with conventional unicast beamforming and without using any CC technique.
- **Multi-user placement, w/o CC:** This scheme employs the memory allocation process proposed in Section III, but data transmission is done with conventional unicast beamforming and without using any CC technique.
- **Multi-user placement, w/ CC:** This scheme employs the memory allocation process proposed in Section III, together with the location-dependent CC delivery scheme in Algorithm 3;
- **Uniform placement, w/ CC:** This scheme employs the conventional uniform memory allocation together with the CC delivery scheme proposed in [42] based on shared caching idea.

In all of these schemes, we use the shared caching approach described in [42] to construct a proper PDA, satisfying the conditions outlined in Definition 1 (as well as Definition 2 for location-dependent CC schemes).

All schemes are compared in terms of their delivery times for 500 random user drops and the resulting cumulative distribution functions (CDF) are shown in Fig. 3. As shown, the scheme with uniform placement has the worst variation in total delivery time, making it unsuitable for applications with real-time content requests (e.g., XR gaming). This variation occurs because uniform placement only maximizes the minimum global caching gain, leading to optimal performance when all users have good connectivity but poor performance when some users experience poor connectivity in bottleneck areas. A location-dependent placement (even without any CC technique) can avoid this issue and improve overall performance. Furthermore, we observe that when no CC technique is used, single-user placement outperforms multi-user placement

due to its higher local-caching gain. However, single-user placement is unsuitable for multicast CC transmission as it does not allocate any cache to the content requested in locations with good connectivity, reducing the possibility of achieving any coded caching gain. Finally, the proposed CC-based transmission scheme with multi-user placement provides the best performance as it enables a global caching gain while also avoiding wireless connectivity bottleneck areas.

Figure 4 compares the performance of different schemes for various values of σ , which controls the attenuation intensity in different STUs. For small σ , the traditional uniform-placement method performs just as well as the proposed CC scheme with multi-user placement, and sometimes even better. This is because, with small σ , the variation in large-scale fading among STUs is small, and hence, non-uniform memory allocation is unnecessary since it reduces the minimum achievable coded caching gain. However, the proposed scheme is more effective (outperforming all other schemes) for larger σ , as there are more attenuated STUs with significant rate differences to well-conditioned STUs. In fact, in these cases, the rate improvement for individual users outweighs the DoF loss caused by the memory allocation process ($K\hat{m} + L$ vs $K\frac{M}{S} + L$ for the uniform placement case).

Figure 5 compares different scheme based on the SNR value at the room border. As depicted, the single-user cache placement scheme is the best option when the received SNR is very low. In this case, the achievable rate at different locations is highly diverse, making the local caching gain the most influential factor in reducing the overall delivery time. Conversely, when the transmit power is high enough to make all locations have similar achievable rates, coded caching gain is the primary factor in reducing the overall transmission time. Therefore, uniform placement is optimal as it maximizes the minimum achievable DoF.

Finally, Figure 6 compares different schemes for a different number of transmit antennas (L). Results show that when L is large, the coded caching gain is less effective in improving overall performance since L is the main contributor to the achievable DoF, i.e., $K\hat{m} + L$. Thus, location-dependent schemes with no CC techniques perform almost as well as the proposed method with multicast CC transmission. However, when L is relatively small, the coded caching gain is crucial in reducing the transmission time, and the proposed scheme is much more effective than the single-user cache placement case. Figures 7 and 8 support a similar conclusion: Figure 7 illustrates that the local caching gain is the most influential factor in reducing delivery time when the available memory is small. This is because the CC gain $K\hat{m}$ is much less than the number of transmit antennas (L) in such scenarios. Figure 8 shows that the performance gap between the proposed method and the rest widens as the number of users increases due to higher achievable CC gain ($K\hat{m}$) for larger K .

VI. CONCLUSION

In this paper, we have proposed a cache placement and delivery scheme for location-dependent data requests suitable for future collaborative wireless XR applications. Our scheme

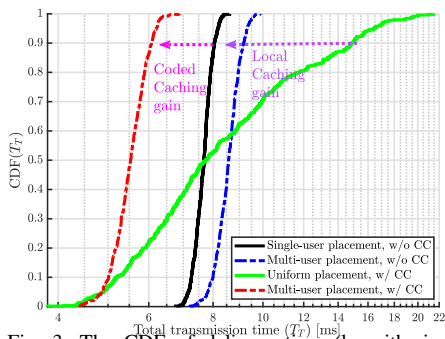


Fig. 3: The CDF of delivery time (logarithmic-scale) for $K = 36$, $M/S = 0.33$, $L = 6$ and $\sigma = 7$.

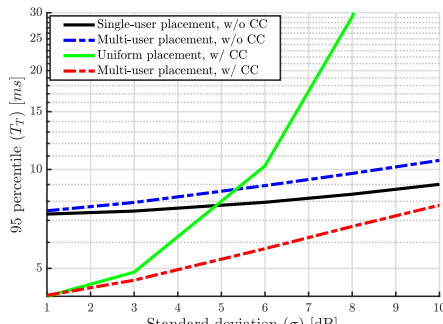


Fig. 4: Delivery time (logarithmic-scale) versus σ , where $K = 36$, $M/S = 0.33$, and $L = 6$.

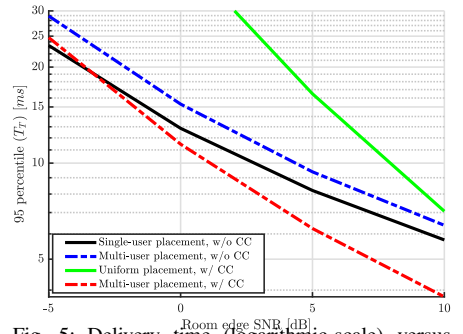


Fig. 5: Delivery time (logarithmic-scale) versus different room edge SNR, where $K = 36$, $M/S = 0.33$, $\sigma = 7$, and $L = 6$.

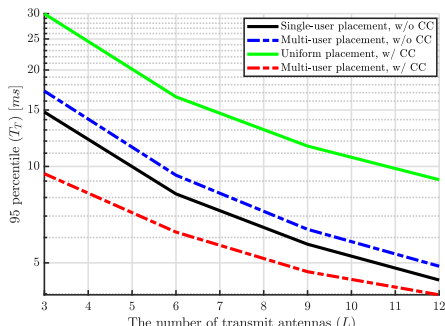


Fig. 6: Delivery time (logarithmic-scale) the number of antennas (L), where $K = 36$, $M/S = 0.33$, and $\sigma = 7$ [dB].

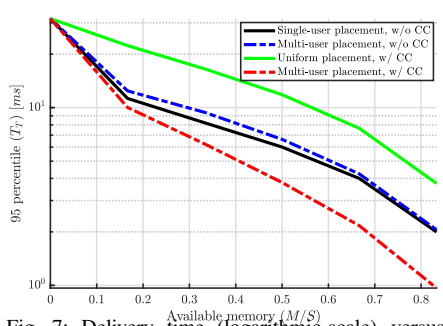


Fig. 7: Delivery time (logarithmic-scale) versus memory size (M/S), where $K = 36$, $\sigma = 7$, and $L = 6$.

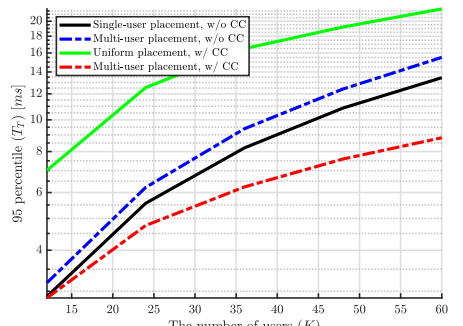


Fig. 8: Delivery time (logarithmic-scale) versus user count (K), where $M/S = 0.33$, $\sigma = 7$, and $L = 6$.

mitigates excessive delivery times through an efficient memory allocation process. We allocate a large portion of memory to bottleneck areas by approximating a rate difference between various locations in the application hall. Due to its simple transceiver design, reduced subpacketization and processing requirements, and the ability to employ shared caching concepts, the proposed scheme can be easily implemented in large networks with many users utilizing a well-defined LAPDA structure. Numerical results demonstrated the superiority of the proposed approach in different scenarios, especially those with high channel variations and a large number of users, for which a bounded transmission time was ensured by minimizing the use of wireless resources in bottleneck areas. In the future, the proposed approach could be extended to include multiple transmitters, incorporate side information regarding user movements and STU transition probabilities, and examine more dynamic scenarios where users' cache content is updated as they navigate through the environment.

APPENDIX A FM MATRIX FORMATION

Section IV introduces the mapping process from RIS \mathcal{N}_k to the TIS $\tilde{\mathcal{N}}_k$ to serve user k appropriately. To facilitate this mapping, K MF matrices \mathbf{G}_k are defined. The element $g_{i,j,k}$ in \mathbf{G}_k specifies the number of file fragments $\{W_j^q(s_k), j \in \mathcal{N}_k, q \in [D_k]\}$ that should be substituted for the temporary index $i \in \tilde{\mathcal{N}}_k$. According to Algorithm 3 for the delivery process, the content transmitted with temporary index $i \in \tilde{\mathcal{N}}_k$ during transmission $n \in [\tilde{N}]$ must be cached by all users $k \in \bar{\mathcal{U}}_i(n)$, where $\bar{\mathcal{U}}_i(n) := \{k \mid k \in \mathcal{U}(n), \hat{\mathbf{Q}}(i, k) = *\}$.

On the other hand, based on the cache placement described in section III, sub-file $W_j(s_k)$ is cached by all users $k \in \mathcal{U}_j(s)$, where $\mathcal{U}_j(s) := \{k \mid k \in [K], \mathbf{Q}_s(j, k) = *\}$. Hence, the value of $g_{i,j,k}$ is determined as follows:

$$\begin{cases} g_{i,j,k} \geq 0, & \text{if } \bar{\mathcal{U}}_i(n) \subseteq \mathcal{U}_j(s_k), \quad \forall k \in [K], \forall i \in \tilde{\mathcal{N}}_k, \\ g_{i,j,k} = 0, & \text{otherwise} \quad \forall j \in \mathcal{N}_k. \end{cases}$$

In cases where $\bar{\mathcal{U}}_i(n) \not\subseteq \mathcal{U}_j(s_k)$ for some $j \in \mathcal{N}_k$ and $i \in \tilde{\mathcal{N}}_k$, it means that there is at least one user in the set $\bar{\mathcal{U}}_i(n)$ who does not have $W_j^q(s_k)$ in its cache. This violation of condition C.4 in Definition 1 results in interference-limited transmission. Consequently, for such cases, no file fragment $W_j^q(s_k)$ should be substituted for the delivery index $i \in \tilde{\mathcal{N}}_k$, i.e., $g_{i,j,k} = 0$.

Next, as discussed in section IV, the total number of file-fragments substituted for a temporary index $i \in \tilde{\mathcal{N}}_k$ must be equal to α . Thus, the non-zero variables $g_{i,j,k}$ must satisfy the following

$$\sum_{j \in \mathcal{N}_k} g_{i,j,k} = \alpha, \quad \forall k \in [K], \forall i \in \tilde{\mathcal{N}}_k. \quad (21)$$

Additionally, the total number of file fragments for each sub-file $W_j(s_k)$ is equal to D_k . Therefore, the total number of file fragments $\{W_j^q(s_k), j \in \mathcal{N}_k\}$ substituted for different temporary indexes $\{i \mid \bar{\mathcal{U}}_i(n) \subseteq \mathcal{U}_j(s_k), i \in \tilde{\mathcal{N}}_k\}$ should sum up to D_k . In other words,

$$\sum_{i \in \tilde{\mathcal{N}}_k} g_{i,j,k} = D_k, \quad \forall k \in [K], \forall j \in \mathcal{N}_k. \quad (22)$$

Consequently, to form each user-specific matrix \mathbf{G}_k , the server needs to solve the non-zero variables $\{g_{i,j,k}\}$, satisfying $\bar{F} - \hat{Z}$ conditions in (21) and $F_{s_k} - Z_{s_k}$ conditions in (22). Hence, to

form the matrix \mathbf{G}_k , the server needs to solve the following system of equations

$$\mathbf{A}_k \mathbf{y} = \mathbf{b}_k, \quad (23)$$

where, $\mathbf{A}_k \in \{0,1\}^{\varphi_k \times \psi_k}$ is the coefficient matrix, $\varphi_k = \hat{F} + F_{s_k} - (\hat{Z} + Z_{s_k})$ is the total number of conditions in (21) and (22), ψ_k is the total number of non-zero variables, $\mathbf{y} \in \mathbb{W}^{\psi_k}$ is the variable vector, and $\mathbf{b}_k \in \{\alpha, D_k\}^{\varphi_k}$ is the target vector. Based on each user state s_k , variable \mathbf{y} in (23) is given in one of the following closed-form [58]

- 1) Over-determined case ($\text{Rank}(\mathbf{A}_k) = \varphi_k$) :

$$\mathbf{y} = (\mathbf{A}_k^T \mathbf{A}_k)^{-1} \mathbf{A}_k^T \mathbf{b}_k,$$

- 2) Under-determined case ($\text{Rank}(\mathbf{A}_k) = \psi_k$) :

$$\mathbf{y} = \mathbf{A}_k^T (\mathbf{A}_k \mathbf{A}_k^T)^{-1} \mathbf{b}_k + (\mathbf{I} - \mathbf{A}_k^T (\mathbf{A}_k \mathbf{A}_k^T)^{-1} \mathbf{A}_k) \mathbf{y}_0,$$

In case $\text{Rank}(\mathbf{A}_k) < \min\{\varphi_k, \psi_k\}$, there are several methods (e.g., singular value decomposition and rank decomposition [58]) available to solve (23), which are beyond the scope of this study. It is worth noting that Definition 2 ensures that there is at least one $g_{i,j,k} > 0$ for every $i \in \mathcal{N}_k$ in equation (21), and similarly for every $j \in \mathcal{N}_k$ in equation (22). Consequently, these equalities remain valid at all times, and equation (23) has a solution that is not empty.

APPENDIX B

NON-INTEGGER CODED CACHING GAINS

We follow a similar memory-sharing scheme as in [19] for non-integer *coded caching* gains (i.e., in case $Km(s)$ is not an integer). In this regard:

1. File $W(s)$ of state s is first divided into two non-overlapping parts $W_1(s)$ and $W_2(s)$, where $|W_1(s)| = (\lfloor Km(s) \rfloor + 1 - Km(s)) |W(s)|$ and $|W_2(s)| = (Km(s) - \lfloor Km(s) \rfloor) |W(s)|$.
2. Two separate MLPDAs $\overline{\mathbf{Q}}(s)$ and $\underline{\mathbf{Q}}(s)$ are formed based on Definition 1, such that $\frac{\overline{Z}(s)}{\overline{F}(s)} = \overline{m}(s) = \frac{\lfloor Km(s) \rfloor + 1}{K}$ and $\frac{\underline{Z}(s)}{\underline{F}(s)} = \underline{m}(s) = \frac{\lfloor Km(s) \rfloor}{K}$.
3. Each user caches the data part $W_1(s)$ based on $\underline{\mathbf{Q}}(s)$, and data part $W_2(s)$ based on $\overline{\mathbf{Q}}(s)$, according to the placement scheme in section III.

It can be verified that the proposed memory-sharing process does not violate the cache constraint, i.e., $\frac{\lfloor Km(s) \rfloor}{K} (\lfloor Km(s) \rfloor + 1 - Km(s)) + \frac{\lfloor Km(s) \rfloor + 1}{K} (Km(s) - \lfloor Km(s) \rfloor) = \frac{Km(s)}{K} = m(s)$.

In this case, the delivery will be done in two sub-phases based on time-sharing. In the first sub-phase, $\beta_1 = (\lfloor Km(s_{k^*}) \rfloor + 1 - Km(s_{k^*}))$ portion of the files are delivered based on $\hat{\mathbf{Q}}_1 \equiv \underline{\mathbf{Q}}(s_{k^*})$, where $k^* = \min_{k \in \mathcal{K}} m_k$. The remaining $\beta_2 = (Km(s_{k^*}) - \lfloor Km(s_{k^*}) \rfloor)$ portion of files are delivered in the second sub-phase based on $\hat{\mathbf{Q}}_2 \equiv \overline{\mathbf{Q}}(s_{k^*})$. We consider two cases for data delivery, 1) $\lfloor Km(s_k) \rfloor > \lfloor Km(s_{k^*}) \rfloor$ and 2) $\lfloor Km(s_k) \rfloor = \lfloor Km(s_{k^*}) \rfloor$.

Case 1 ($\lfloor \mathbf{K}\mathbf{m}(s_k) \rfloor > \lfloor \mathbf{K}\mathbf{m}(s_{k^*}) \rfloor$): Since in this case, for all user k , the placement is done differently for $W_1(s_k)$ and $W_2(s_k)$, the index mapping process is also separately performed for $W_1(s_k)$ and $W_2(s_k)$. To this end, during the first delivery sub-phase, β_1 portion of every *sub-file* of $W_1(s_k)$

is divided into $\underline{D}_k^1 = \frac{\alpha \underline{F} - \underline{Z}}{\underline{F}_{s_k} - \underline{Z}_{s_k}}$ smaller fragments, where \underline{F} and \underline{Z} are equivalent to $\underline{F}_{s_{k^*}}$ and $\underline{Z}_{s_{k^*}}$, respectively. Similarly, β_1 portion of every *sub-file* of $W_2(s_k)$ is divided into and $\underline{D}_k^2 = \frac{\alpha \overline{F} - \overline{Z}}{\overline{F}_{s_k} - \overline{Z}_{s_k}}$ smaller fragments. Then, based on $\hat{\mathbf{Q}}_1$, $\underline{\mathbf{Q}}(s_k)$, and $\overline{\mathbf{Q}}(s_k)$, two file-fragment matrices $\underline{\mathbf{P}}_k^1$ and $\overline{\mathbf{P}}_k^2$ are formed for $W_1(s_k)$ and $W_2(s_k)$, respectively. Using $\underline{\mathbf{P}}_k^1$ and $\overline{\mathbf{P}}_k^2$, each transmitted message to user k will carry $\underline{\alpha}$ file-fragments of β_1 portion of $W_1(s_k)$ and $\underline{\alpha}$ file-fragments of β_1 portion of $W_2(s_k)$. The remaining β_2 portion of $W_1(s_k)$ and $W_2(s_k)$ will be delivered in the second sub-phase, using $\hat{\mathbf{Q}}_2$, $\underline{\mathbf{Q}}(s_k)$, and $\overline{\mathbf{Q}}(s_k)$ to form $\overline{\mathbf{P}}_k^1$ and $\overline{\mathbf{P}}_k^2$. For the sake of brevity, we avoid reviewing a similar process in the second delivery sub-phase.

Case 2 ($\lfloor \mathbf{K}\mathbf{m}(s_k) \rfloor = \lfloor \mathbf{K}\mathbf{m}(s_{k^*}) \rfloor$): In this case, $(\lfloor Km(s_k) \rfloor + 1 - Km(s_k))$ portion of $W(s_k)$ (i.e., $W_1(s_k)$) is already cached based on $\hat{\mathbf{Q}}_1$ and can be easily delivered by forming $\underline{\mathbf{P}}_k^1$. The remaining $\beta_1 - (\lfloor Km(s_k) \rfloor + 1 - Km(s_k))$ portion of $W(s_k)$ can also be delivered in the first delivery sub-phase based on $\hat{\mathbf{Q}}_1$ and $\overline{\mathbf{Q}}(s_k)$. In this regard, $\beta_1 - (\lfloor Km(s_k) \rfloor + 1 - Km(s_k))$ portion of every *sub-file* of $W_2(s_k)$ is divided into and $\underline{D}_k^2 = \frac{\alpha \overline{F} - \overline{Z}}{\overline{F}_{s_k} - \overline{Z}_{s_k}}$ smaller fragments. Then, using $\underline{\mathbf{P}}_k^1$ and $\overline{\mathbf{P}}_k^2$, each transmitted message to user k will carry $\underline{\alpha}$ file-fragments of $W_1(s_k)$ and $\underline{\alpha}$ file-fragments of $\beta_1 - (\lfloor Km(s_k) \rfloor + 1 - Km(s_k))$ portion of $W_2(s_k)$. In the second sub-phase, the remaining portion of $W(s_k)$, i.e., $(\lfloor Km(s_k) \rfloor - \lfloor Km(s_k) \rfloor) - (\beta_1 - (\lfloor Km(s_k) \rfloor + 1 - Km(s_k))) = 1 - \beta_1 = \beta_2$ portion of $W_2(s_k)$, will be delivered based on $\hat{\mathbf{Q}}_2$ and $\overline{\mathbf{Q}}(s_k)$.

REFERENCES

- [1] Cisco, "Cisco Annual Internet Report, 2018–2023," *White Paper*, vol. 1, march, 2020.
- [2] M. Salehi, K. Hooli, J. Hulkkonen, and A. Tölli, "Enhancing next-generation extended reality applications with coded caching," *IEEE Open Journal of the Communications Society*, 2023.
- [3] K. Boos, D. Chu, and E. Cuervo, "Flashback: Immersive virtual reality on mobile devices via rendering memoization," in *Proceedings of the 14th Annual International Conference on Mobile Systems, Applications, and Services*, 2016, pp. 291–304.
- [4] E. Thomas, E. Potetsianakis, T. Stockhammer, I. Bouazizi, and M.-L. Champel, "MPEG Media Enablers For Richer XR Experiences," *arXiv*, 2020. [Online]. Available: <https://arxiv.org/abs/2010.04645>.
- [5] N. Rajatheva, I. Atzeni, E. Bjornson, A. Bourdoux, S. Buzzi, J.-B. Dore, S. Erkucuk, M. Fuentes, K. Guan, Y. Hu et al., "White paper on broadband connectivity in 6G," *arXiv preprint arXiv:2004.14247*, 2020.
- [6] E. Bastug, M. Bennis, M. Médard, and M. Debbah, "Toward interconnected virtual reality: Opportunities, challenges, and enablers," *IEEE Communications Magazine*, vol. 55, no. 6, pp. 110–117, 2017.
- [7] T. Taleb, A. Boudi, L. Rosa, L. Cordeiro, T. Theodoropoulos, K. Tserpes, P. Dazzi, A. Protopsaltis, and R. Li, "Towards supporting XR services: Architecture and enablers," *IEEE Internet of Things Journal*, 2022.
- [8] C. Chaccour, M. N. Soorki, W. Saad, M. Bennis, and P. Popovski, "Can terahertz provide high-rate reliable low latency communications for wireless vr?" *IEEE Internet of Things Journal*, 2022.
- [9] M. Chen, W. Saad, and C. Yin, "Virtual reality over wireless networks: Quality-of-service model and learning-based resource management," *IEEE Transactions on Communications*, vol. 66, no. 11, pp. 5621–5635, 2018.
- [10] G. Pocovi, B. Soret, K. I. Pedersen, and P. Mogensen, "MAC layer enhancements for ultra-reliable low-latency communications in cellular networks," in *2017 IEEE International Conference on Communications Workshops (ICC Workshops)*. IEEE, 2017, pp. 1005–1010.

- [11] H. Liu, Z. Chen, and L. Qian, "The three primary colors of mobile systems," *IEEE Comm. Mag.*, vol. 54, no. 9, pp. 15–21, 2016.
- [12] G. S. Paschos, G. Iosifidis, M. Tao, D. Towsley, and G. Caire, "The role of caching in future communication systems and networks," *IEEE Journal on Selected Areas in Communications*, vol. 36, no. 6, pp. 1111–1125, 2018.
- [13] Y. Sun, Z. Chen, M. Tao, and H. Liu, "Communications, caching, and computing for mobile virtual reality: Modeling and tradeoff," *IEEE Transactions on Communications*, vol. 67, no. 11, pp. 7573–7586, 2019.
- [14] X. Yang, Z. Chen, K. Li, Y. Sun, N. Liu, W. Xie, and Y. Zhao, "Communication-constrained mobile edge computing systems for wireless virtual reality: Scheduling and tradeoff," *IEEE Access*, vol. 6, pp. 16 665–16 677, 2018.
- [15] Y. Sun, Z. Chen, M. Tao, and H. Liu, "Bandwidth gain from mobile edge computing and caching in wireless multicast systems," *IEEE Trans. on Wireless Comm.*, vol. 19, no. 6, pp. 3992–4007, 2020.
- [16] T. Dang and M. Peng, "Joint radio communication, caching, and computing design for mobile virtual reality delivery in fog radio access networks," *IEEE Journal on Selected Areas in Communications*, vol. 37, no. 7, pp. 1594–1607, 2019.
- [17] E. Bastug, M. Bennis, and M. Debbah, "Living on the edge: The role of proactive caching in 5G wireless networks," *IEEE Communications Magazine*, vol. 52, no. 8, pp. 82–89, 2014.
- [18] C. Yang, Y. Yao, Z. Chen, and B. Xia, "Analysis on cache-enabled wireless heterogeneous networks," *IEEE Transactions on Wireless Communications*, vol. 15, no. 1, pp. 131–145, 2015.
- [19] M. A. Maddah-Ali and U. Niesen, "Fundamental limits of caching," *IEEE Trans. Inform. Theory*, vol. 60, no. 5, pp. 2856–2867, May 2014.
- [20] Y. Li, Z. Chen, and M. Tao, "Coded caching with device computing in mobile edge computing systems," *IEEE Transactions on Wireless Communications*, 2021.
- [21] H. B. Mahmoodi, M. Salehi, and A. Tölili, "Non-symmetric coded caching for location-dependent content delivery," in *2021 IEEE International Symposium on Information Theory (ISIT)*, 2021, pp. 712–717.
- [22] H. B. Mahmoodi, M. J. Salehi, and A. Tölili, "Asymmetric multi-antenna coded caching for location-dependent content delivery," in *GLOBECOM 2022-2022 IEEE Glob. Comm. Conf.*, 2022, pp. 1930–1935.
- [23] H. B. Mahmoodi, M. Salehi, and A. Tölili, "Non-symmetric multi-antenna coded caching for location-dependent content delivery," in *JCC 2022-IEEE International Conference on Communications*. IEEE, 2022, pp. 5165–5170.
- [24] H. B. Mahmoodi, M. Salehi, and A. Tölili, "Multi-antenna coded caching for location-dependent content delivery," *IEEE Transactions on Wireless Communications*, pp. 1–1, 2023.
- [25] S. P. Shariatpanahi, G. Caire, and B. Hossein Khalaj, "Physical-layer schemes for wireless coded caching," *IEEE Trans. Inform. Theory*, vol. 65, no. 5, pp. 2792–2807, 2019.
- [26] S. P. Shariatpanahi *et al.*, "Multi-server coded caching," *IEEE Trans. Inform. Theory*, vol. 62, no. 12, pp. 7253–7271, Dec 2016.
- [27] Q. Yu, M. A. Maddah-Ali, and A. S. Avestimehr, "The exact rate-memory tradeoff for caching with uncoded prefetching," *IEEE International Symposium on Information Theory - Proceedings*, vol. 64, no. 2, pp. 1613–1617, 2017.
- [28] A. Tölili, S. P. Shariatpanahi, J. Kaleva, and B. H. Khalaj, "Multi-antenna interference management for coded caching," *IEEE Transactions on Wireless Communications*, vol. 19, no. 3, pp. 2091–2106, 2020.
- [29] M. Ji, G. Caire, and A. F. Molisch, "Fundamental limits of caching in wireless D2D networks," *IEEE Trans. Inform. Theory*, vol. 62, no. 2, pp. 849–869, Feb 2016.
- [30] C. Yapar, K. Wan, R. F. Schaefer, and G. Caire, "On the optimality of D2D coded caching with uncoded cache placement and one-shot delivery," *IEEE Trans. Commun.*, vol. 67, no. 12, pp. 8179–8192, 2019.
- [31] H. B. Mahmoodi, J. Kaleva, S. P. Shariatpanahi, and A. Tölili, "D2D assisted multi-antenna coded caching," *IEEE Access*, vol. 11, pp. 16 271–16 287, 2023.
- [32] Q. Yan, M. Cheng, X. Tang, and Q. Chen, "On the placement delivery array design for centralized coded caching scheme," *IEEE Transactions on Information Theory*, vol. 63, no. 9, pp. 5821–5833, 2017.
- [33] M. Cheng, J. Jiang, Q. Wang, and Y. Yao, "A generalized grouping scheme in coded caching," *IEEE Transactions on Communications*, vol. 67, no. 5, pp. 3422–3430, 2019.
- [34] J. Wang, M. Cheng, Q. Yan, and X. Tang, "Placement delivery array design for coded caching scheme in D2D networks," *IEEE Trans. Commun.*, vol. 67, no. 5, pp. 3388–3395, May 2019.
- [35] M. Cheng, J. Wang, X. Zhong, and Q. Wang, "A framework of constructing placement delivery arrays for centralized coded caching," *IEEE Transactions on Information Theory*, vol. 67, no. 11, pp. 7121–7131, 2021.
- [36] E. Lampsiris and P. Elia, "Adding transmitters dramatically boosts coded-caching gains for finite file sizes," *IEEE Journal on Selected Areas in Communications*, vol. 36, no. 6, pp. 1176–1188, 2018.
- [37] E. Parrinello, A. Ünsal, and P. Elia, "Fundamental limits of coded caching with multiple antennas, shared caches and uncoded prefetching," *IEEE Transactions on Information Theory*, vol. 66, no. 4, pp. 2252–2268, 2020.
- [38] M. Dutta and A. Thomas, "Decentralized coded caching for shared caches," *IEEE Comm. Letters*, vol. 25, no. 5, pp. 1458–1462, 2021.
- [39] M. J. Salehi, H. B. Mahmoodi, and A. Tölili, "A Low-Subpacketization High-Performance MIMO Coded Caching Scheme," in *WSA 2021 - 25th International ITG Workshop on Smart Antennas*, 2021, pp. 427–432.
- [40] M. Salehi, M. Naseri-Tehrani, and A. Tölili, "Multicast beamformer design for MIMO coded caching systems," in *ICASSP 2023-2023 IEEE International Conference on Acoustics, Speech and Signal Processing (ICASSP)*. IEEE, 2023, pp. 1–5.
- [41] M. Abolpour, M. J. Salehi, and A. Tolli, "Coded Caching and Spatial Multiplexing Gain Trade-off in Dynamic MISO Networks," *IEEE Workshop on Signal Processing Advances in Wireless Communications, SPAWC*, vol. 2022-July, 2022.
- [42] M. Abolpour, M. Salehi, and A. Tölili, "Cache-aided communications in MISO networks with dynamic user behavior: A universal solution," in *2023 IEEE Int. Symp. on Inf. Theory (ISIT)*, available at: [arXiv:2304.11623](https://arxiv.org/abs/2304.11623), 2023.
- [43] M. Salehi, E. Parrinello, H. B. Mahmoodi, and A. Tölili, "Low-subpacketization multi-antenna coded caching for dynamic networks," in *2022 Joint European Conference on Networks and Communications & 6G Summit (EuCNC/6G Summit)*. IEEE, 2022, pp. 112–117.
- [44] T. Yang, K. Wan, M. Cheng, R. C. Qiu, and G. Caire, "Multiple-antenna placement delivery array for cache-aided miso systems," *IEEE Transactions on Information Theory*, 2023.
- [45] M. Salehi, A. Tolli, S. P. Shariatpanahi, and J. Kaleva, "Subpacketization-rate trade-off in multi-antenna coded caching," in *2019 IEEE Global Communications Conference, GLOBECOM 2019 - Proceedings*. IEEE, 2019, pp. 1–6.
- [46] M. Salehi and A. Tölili, "Multi-antenna Coded Caching at Finite-SNR: Breaking Down the Gain Structure," *arXiv preprint arXiv:2210.10433*, 2022.
- [47] H. Zhao, A. Bazco-Nogueras, and P. Elia, "Resolving the worst-user bottleneck of coded caching: Exploiting finite file sizes," in *2020 IEEE Information Theory Workshop (ITW)*. IEEE, 2021, pp. 1–5.
- [48] A. Destounis, A. Ghorbel, G. S. Paschos, and M. Kobayashi, "Adaptive Coded Caching for Fair Delivery over Fading Channels," *IEEE Transactions on Information Theory*, 2020.
- [49] Y. Gu, C. Yang, B. Xia, and D. Xu, "Design and analysis of coded caching schemes in stochastic wireless networks," *IEEE Transactions on Wireless Communications*, 2021.
- [50] Y. Liu, A. Tang, and X. Wang, "Joint scheduling and power optimization for delay constrained transmissions in coded caching over wireless fading channels," *IEEE Transactions on Wireless Communications*, 2021.
- [51] M. Salehi, A. Tolli, and S. P. Shariatpanahi, "Coded caching with uneven channels: A quality of experience approach," in *2020 IEEE Int. Workshop on Sig. Proc. Advances in Wireless Comm. (SPAWC)*, 2020, pp. 1–5.
- [52] M. A. Maddah-Ali and U. Niesen, "Fundamental limits of caching," *IEEE Trans. on Inf. Theory*, vol. 60, no. 5, pp. 2856–2867, 2014.
- [53] M. Salehi, E. Parrinello, S. P. Shariatpanahi, P. Elia, and A. Tölili, "Low-complexity high-performance cyclic caching for large MISO systems," *IEEE Transactions on Wireless Communications*, vol. 21, no. 5, pp. 3263–3278, 2022.
- [54] A. Tang, S. Roy, and X. Wang, "Coded caching for wireless backhaul networks with unequal link rates," *IEEE Transactions on Communications*, vol. 66, no. 1, pp. 1–13, 2017.
- [55] H. Zhao, A. Bazco-Nogueras, and P. Elia, "Wireless coded caching with shared caches can overcome the near-far bottleneck," in *2021 IEEE Int. Symp. on Inf. Theory (ISIT)*, 2021, pp. 350–355.
- [56] —, "Coded caching gains at low SNR over nakagami fading channels," in *Proc. 55th Asilomar Conf. Signals, Syst., Comput.(ACSSC)*, 2021.
- [57] E. Parrinello, A. Ünsal, and P. Elia, "Fundamental Limits of Coded Caching with Multiple Antennas, Shared Caches and Uncoded Prefetching," *IEEE Transactions on Information Theory*, 2019.
- [58] H. Anton, *Elementary Linear Algebra*. New York, USA: John Wiley, 1987.